ACS APPLIED MATERIALS & INTERFACES

Research Article

www.acsami.org

Unveiling the Hard Anodization Regime of Aluminum: Insight into the Nanopore Self-Organization and Growth Mechanism

Víctor Vega,[*,†,‡] Javier García,[§,⊥] Josep M. Montero-Moreno,[§] Blanca Hernando,[†] Julien Bachmann,[∥] Víctor. M. Prida,[†] and Kornelius Nielsch[§,⊥]

[†]Departamento de Física, Universidad de Oviedo, Calvo Sotelo s/n, 33007-Oviedo, Asturias Spain

[‡]Laboratorio de Membranas Nanoporosas, Universidad de Oviedo, Edif. Severo Ochoa, Campus del Cristo s/n. 33006-Oviedo, Asturias Spain

[§]Institut für Angewandte Physik, Universität Hamburg, Jungiusstraße 11, 20355-Hamburg, Germany

[∥]Department of Chemistry and Pharmacy, Friedrich-Alexander-University, Erlangen-Nürnberg, Egerlandstraße 1, 91058-Erlangen, Germany

Supporting Information

ABSTRACT: The pore growth mechanism and its self-ordering conditions are investigated for nanoporous alumina membranes synthesized by hard anodization (HA) of Al in a broad range of anodic conditions, covering oxalic acid electrolytes with concentrations from 0.300 M down to 0.075 M and potentiostatic anodization voltages between 120 and 225 V. The use of linear sweep voltammetry (LSV) and scanning and transmission electron microscopy, together with image analysis techniques allow one to characterize the intrinsic nature of the HA regime. HA of aluminum is explained on the basis of a phenomenological model taking into account the role of oxalate ions and their limited diffusion through alumina nanochannels from a bulk electrolyte. The depletion of oxalate ions at the bottom of the pores causes an increased growth of the alumina barrier layer at the oxide/electrolyte interface. Furthermore, an innovative method has been developed for the determination of the HA conditions leading to self-ordered pore growth in any given electrolyte, thus allowing one to extend the available range of interpore distances of the highly ordered hexagonal pore arrangement in a wide range of 240−507 nm, while keeping small pore diameters of 50−60 nm.

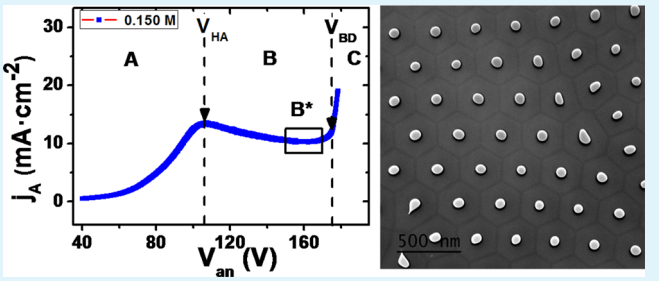

KEYWORDS: *hard anodization, self-organization, diffusion limited reaction, anodic aluminum oxide, nanoporous alumina*

INTRODUCTION

The novel opportunity of synthesizing self-ordered nanoporous anodic aluminum oxide (AAO) membranes with a high quality of the hexagonal pore arrangement by means of hard anodization (HA) has drawn a renewed interest in the development of innovative applications for such nanoporous structures, as well as to the spread of the current applications in conventional mild anodization (MA) to this new kind of nanoporous alumina templates. The intrinsic characteristics of this outstanding electrochemical fabrication method, such as its short processing time (1−5 h compared to the 24 to 48 h typical for the MA), high throughput, enhanced chemical and mechanical properties, and large range of available self-ordering conditions,[1,2] can be advantageous when compared with those of MA.

The short processing times necessary for the fabrication of hard anodic aluminum oxide (H-AAO) membranes arise from the fast nanoporous oxide growth rates of about 40 up to 80 $\mu m \cdot h^{-1}$ compared to the 1 up to 3 $\mu m \cdot h^{-1}$ obtained for conventional mild anodic aluminum oxide (M-AAO) grown in oxalic acid electrolytes under similar temperature conditions. In addition, it is remarkable that there is a possibility of obtaining high quality self-ordered pore arrangements in a fast single HA step,[2−4] contrary to the well-established two-step MA process,[5] which needs a long first anodization step in order to develop a highly ordered pore arrangement. Finally, nanoporous AAO membranes exhibiting well-ordered porous structures through the whole membrane thickness can also be obtained by a two-step approach under some specific HA conditions or by a combination with suitable mild anodization.[6,7] HA methods also provide the possibility of obtaining a wider range of interpore distances within the self-organized pore regime than those obtained in M-AAO. Indeed, interpore distance values between 70 and 450 nm are achievable by HA using appropriate anodizing electrolytic baths.[8,9] H-AAO membranes display some interesting additional features that provide extra freedom degrees for the manufacture of patterned templates with tunable geometries. It has been reported that not only the

Received: November 6, 2015
Accepted: December 8, 2015

ACS Publications © XXXX American Chemical Society

DOI: 10.1021/acsami.5b10712
ACS Appl. Mater. Interfaces XXXX, XXX, XXX−XXX

anodization voltage but also the anodization current density exerts a significant influence on modifying the alumina barrier layer thickness, pore diameter, interpore distance, and spatial periodic ordering degree of the close-packed nanopore arrangement.[2,8,10] The ability to control these parameters independently may confer a high versatility to this process with respect to MA in order to tune all geometrical parameters of the AAO at will and in a much wider range. Recently, we have successfully applied the HA process in combination with interference lithography to produce perfectly ordered AAO membranes, demonstrating that the versatility of the HA was crucial to achieving perfect pore arrangement through large surface area membranes.[11] Additionally, it has been shown that HA can be used in combination with MA in sequential or pulsed processes, thus opening the door for the fabrication of new tailor-designed nanomaterials with complex three-dimensional structures.[2,12−21]

Despite the mentioned potential advantages of HA of aluminum in comparison with the conventional MA approach, it presents some disadvantages and technical difficulties, including the high tendency to show dielectric breakdown phenomena and need of high cooling power in order to dissipate the large amount of heat associated with high current densities (as high as 200 mA·cm^{-2}) characteristic of HA. The HA method has been successfully performed in several electrolytes comprising sulfuric[1] and oxalic acids[2] and mixtures between these acids.[8,22] The use of additives such as ethanol[10,15] and aluminum sulfate[23] or oxalate[24] is common, in order to stabilize the anodization process and to avoid the dielectric breakdown of the anodic oxide layer. A complementary and well-established approach is to perform a preanodization step under MA conditions, followed by a linear sweep of the anodization voltage up to reach potentiostatic HA conditions, resulting in flat and smooth H-AAO membranes.[2,4] This prevents the high anodic current densities that appear during the first stages of the HA, which are responsible for local catastrophic burning phenomena.

There is, however, a substantial lack of scientific and technical knowledge about the nature of the HA processes, the nanopore growth mechanism and self-ordering conditions, and the relevant technical possibilities of nanofabrication offered by this novel electrochemical technique. The experimental correlations found in the case of MA between the self-organization of pores, governed by the local electric field, and the geometric parameters of the pores have been missing for HA. A complete understanding of the HA process would facilitate the application of this technique for the fabrication of nanoporous membranes with tailored geometry, which are highly appreciated in nanoscience and nanotechnology for a broad spectrum of applications ranging from chemical and biochemical sensors,[25−28] nanofiltration,[29] drug delivery,[30] superhydrophobic surfaces,[31] and nanogenerators,[32−34] among many others.

In the present work, we report on a systematic study of the HA process and the nanopore self-ordering regime in oxalic acid electrolytes, covering a wide range of anodic conditions (electrolyte concentration and anodic voltage). A detailed characterization of the morphological features of H-AAO membranes is performed as a function of the synthesis conditions, shedding light into the intrinsic nature of HA processes. The analysis of the main features of the anodic oxidation of Al in oxalic acid electrolytes with varying concentration is carried out based on a LSV study performed in a wide voltage range from 40 V up to 250 V, which enables one to determine the HA voltage intervals leading to stable hard anodization conditions. Consequently, a correlation of LSV curves with the self-ordered growth of the nanopore arrangements is determined for the studied electrolytes. In addition, potentiostatic hard anodization experiments have been carried out under different experimental conditions, and the data collected from scanning and transmission electron microscopy characterization, in combination with the analysis of the corresponding anodization current transients, were useful to understand the HA processes. The accurate study presented here, which involves a deep comprehension on the nature of HA processes, along with a careful analysis of the voltammetric curves, could provide a systematic procedure to determine the optimum HA self-ordering interval for other electrolytes, thus allowing for a continuous tuning of the geometrical characteristics of H-AAO membranes.

EXPERIMENTAL SECTION

High purity Al foils (Goodfellow, Al 99.999%), 2.5 cm in diameter and 0.5 mm in thickness, were cleaned by sonication in isopropanol and ethanol. Prior to HA and voltammetric studies, the samples were loaded into a two-electrode anodization cell equipped with a 100 mL electrolyte reservoir, which exposes a sample area of 2.54 cm^2 to the electrolyte. The cell includes a Cu back plate which is used to provide both electrical and thermal contact to the sample and a Pt counter-electrode. The Al foils were then electropolished in a mixture of perchloric acid and ethanol (1:3 vol.) at 5 °C and 20 V. The electropolished Al foils were subsequently anodized under mild anodization conditions during 15 min (0.300 M oxalic acid solution at 40 V and 3 °C). Afterward, the oxalic acid (0.300 M) electrolyte was replaced with a renewed electrolyte having the desired oxalic acid and ethanol concentrations, and the anodization voltage was slowly swept from 40 V to the target HA voltage in the range of 100−250 V. A constant voltage sweep rate of 0.02 V·s^{-1} was employed, unless a different sweep rate is specified in the text. In voltammetric measurements, the voltage was increased at the same sweep rate until the dielectric breakdown of the alumina barrier layer is evidenced by a sudden increase of the anodic current density.

Both, HA processes and voltammetric studies were performed in oxalic acid electrolytes, with concentrations selected in the range between 0.300 ± 0.002 M and 0.075 ± 0.002 M, and containing a certain amount of ethanol (5−10 vol %), which acts as an antifreezing agent and contributes to dissipating the heat generated during the HA processes.[8,10] The concentration of ethanol was selected as the minimum addition that prevents electrolyte freezing, thus avoiding high ethanol concentrations that may deteriorate the quality of the H-AAO membranes.[7] The temperature of the electrolytes was adjusted in the range between −1 to 0 °C prior to the HA step, and it was maintained below 3 °C by an external recirculating bath that refrigerates the copper back plate and the anodic electrode. The electrolytes were vigorously stirred during anodization, in order to ensure the homogeneity of the temperature and bulk electrolyte concentration within the anodization cell during the entire anodization process. The anodization voltages (V_{an}), ranging from 40 to 250 V, were applied between the sample and the Pt counter electrode by a computer controlled power supply, whereas anodization current transients were monitored by means of a computer controlled digital multimeter. The reported values of the anodic current density, j_A, are obtained as the ratio between measured anodic current intensity and the total sample area, without considering the effective area of the porous alumina layer.

After the HA processes, the remaining Al substrate was removed by wet chemical etching in an aqueous solution of 0.14 M $CuCl_2$ and 0.4 M HCl. The alumina barrier layer at the bottom of the pores was removed by reactive ion etching (Sentech, SI 220) from the back of the AAO membranes in a plasma generated from a mixture of O_2 and CF_4 at 12 mTorr under an applied power of 250 W (0.8 W cm^{-2}). The

DOI: 10.1021/acsami.5b10712
ACS Appl. Mater. Interfaces XXXX, XXX, XXX−XXX

morphology of the back of the samples was studied by means of scanning electron microscopy (SEM, Supra 55-Zeiss). The determination of the interpore distance (D_{int}), pore diameters (D_p), and barrier layer thicknesses (t_{BL}) was performed by image analysis of bottom and cross-section view SEM micrographs using the image processing packages ImageJ, version 1.48 (NIH, USA), and WsXM, version 5.0 (Nanotec, Spain).[35,36] The microstructure of some of the samples was studied by TEM after reducing the membrane thickness to few nanometers by ion milling.

RESULTS AND DISCUSSION

A characteristic current transient recorded during the H-AAO fabrication procedure is shown in Figure 1a, whereas some

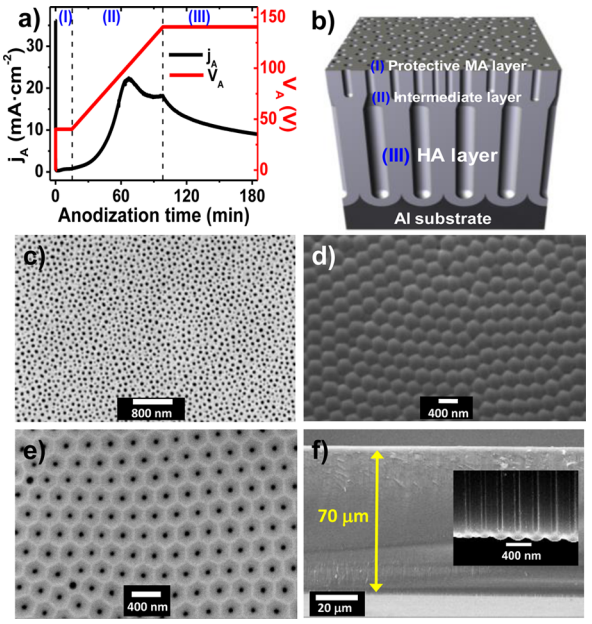

Figure 1. (a) Characteristic current and voltage transients recorded during the fabrication of an H-AAO membrane. (b) Schematic drawing of the H-AAO structure, indicating the protective MA layer at the top, the intermediate layer, and the highly ordered HA layer. (c–f) SEM images of H-AAO membranes. (c) Top view, showing the protective MA layer. (d) Bottom view, showing the high ordering degree in the bottom of the H-AAO. (e) Bottom view after removing the alumina barrier layer which blocks the bottom of the pores. (f) Cross-section view. The inset in f shows a magnification of the region close to the alumina barrier layer, evidencing that the pores grow parallel to each other during the HA process.

relevant SEM images of a H-AAO membrane are shown in Figure 1c–f. Three different stages corresponding to the employed anodization protocol can be distinguished in the current transient of Figure 1a, leading to the growth of three nanoporous layers with different morphologies indicated in Figure 1b. The initial potentiostatic MA step (I), showing the typical current transient, provides a first thick alumina layer with a dense and highly disordered porous structure showing a broad pore size distribution (Figure 1c). This layer acts as a protection for the HA step preventing undesired burning phenomena due to high current density flow. (II) During the linear voltage sweep, the anodization conditions are varied from MA (40 V) to the desired HA voltage (140 V in this particular case). An exponential increase of the current density is observed until a maximum is reached, after which the current decreases. During this step, a rearrangement of the pores takes place in order to accommodate their growth to the continuous change of the anodization voltage.[4] (III) When the final HA voltage is reached and kept constant, a fast decrease of the anodization current density with time is observed. This has been attributed to the rapid increase of the nanopores length, which lengthens the diffusion path of the ionic species involved in the electrochemical reaction.[2,4] During the anodization stage (III), the pores are uniform in size, and they grow parallel to each other, following a highly ordered hexagonal arrangement, as can be observed in Figures 1d and e, and in the inset of Figure 1f. An average growth rate of about 50 μm/h can be roughly estimated from Figure 1f, which corresponds to a cross-section view of a membrane anodized under hard anodization conditions during 1.5 h. This value is reduced to around 25 μm/h when the duration of the whole process, i.e., MA and voltage ramp steps, is taken into account. However, the AAO nanoporous layer growth rate does not keep constant during the entire HA process, and therefore, the H-AAO membrane thickness does not increase linearly with the anodization time, as evidenced in Figure S1 (Supporting Information) and explained in detail in the following sections.

Voltammetric Studies of the Anodic Oxidation of Aluminum. Figure 2a shows a typical LSV measured at a sweep rate of 0.02 V·s^{-1} during the anodic oxidation of Al in a

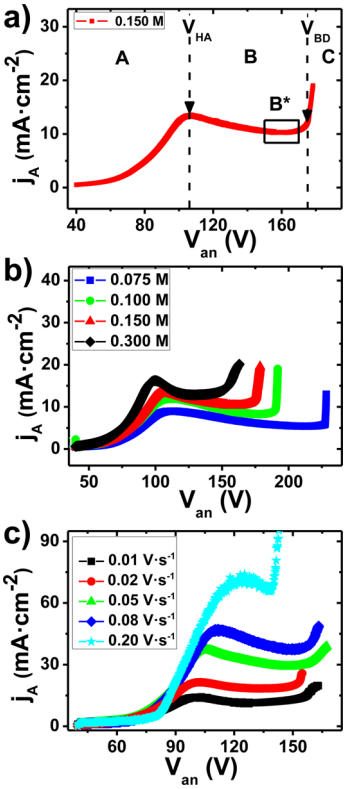

Figure 2. (a) LSV of the anodic oxidation behavior of Al in 0.15 M oxalic acid electrolyte containing 5 vol % of ethanol. The different stages are labeled as A (mild anodization regime), B (hard anodization regime), B* (current plateau), and C (dielectric breakdown). The voltage values V_{HA} and V_{BD} indicate the beginning of the HA regime and the dielectric breakdown of the anodic oxide, respectively. (b) LSV characteristic of the anodic oxidation of Al in several electrolytes with different oxalic acid concentrations ranging from 0.075 to 0.300 M and 5–10 vol % of ethanol. (c) LSV of the anodic oxidation of Al in 0.3 M oxalic acid electrolyte and 5 vol % of ethanol obtained at different voltage sweeping rates.

DOI: 10.1021/acsami.5b10712
ACS Appl. Mater. Interfaces XXXX, XXX, XXX–XXX

0.15 M oxalic acid electrolyte containing 5 vol % of ethanol. Three different regions, respectively labeled as A, B, and C, can be clearly distinguished. In region A, corresponding to low values of the applied anodization voltage (40−106 V), the anodic current density, j_A, increases monotonously with increasing anodization voltage. This current increase is in agreement with the high-field conduction theory well established for MA processes, which relates the anodic current density with the potential drop across the barrier layer, ΔV_{BL}, through eq 1:

$$j_A = j_0 e^{(\beta \Delta V_{BL}/t_{BL})} \quad (1)$$

where t_{BL} the barrier layer thickness. The parameters β and j_0 depend on the material and anodic conditions of the experiment and change with temperature as T^{-1} and $e^{-1/T}$, respectively.[2,20,37−40] Therefore, in region A, which corresponds to the MA regime, the current density is limited by the electric field-driven ion migration across the oxide barrier layer. This expression is also in good agreement with the classical explanation of the current transients during the potentiostatic MA of aluminum, in which the different stages of the anodization process are correlated with changes in the barrier layer thickness due to the competition between oxidation and dissolution processes.[41−43]

The transition between regions A and B in Figure 2a is delimited by the presence of a local maximum of the current density at a certain value of the anodic voltage $V_{an} = V_{HA}$, which can be ascribed to the beginning of the HA regime, as it will be discussed below. Further increases of the anodic voltage result in lower anodic current densities, an indication that the current density-limiting mechanism has changed. In fact, it has been stated that during potentiostatic HA processes, the fast growth of the nanopores causes an exponential current decrease (see Figure 1a). This effect has been related to a diffusion limiting mechanism due to the increasing diffusion length with the pore growth for the ionic species involved in the anodic oxidation of Al.[2−4] However, to the best of our knowledge, a direct experimental demonstration of this interpretation has not yet been shown in the literature so far.

The HA region (labeled as B in Figure 2a) can be considered to extend from V_{HA} up to a certain voltage value, V_{BD}, at which the anodic current density dramatically increases. This is due to the dielectric breakdown of the alumina barrier layer as a result of the high electric field. Dielectric breakdown is accompanied by an intense heat generation causing a catastrophic damage of the nanoporous membrane, ascribed to the following region C. The presence of a current plateau can be also observed in region B of Figure 2a. Therefore, region B^* is defined as a voltage range of 20 to 30 V around the minimum current density value of the plateau region. A similar behavior was observed in electrolytes with different oxalic acid concentrations, ranging from 0.075 to 0.300 M (Figure 2b). The characteristic values of V_{HA}, V_{BD}, and B^* for each electrolyte concentration are displayed in Table 1. The selected value for the voltage sweep rate employed in the LSV experiments (0.02 $V{\cdot}s^{-1}$ in all of the previous measurements) can also modify the resulting curves. The effect of employing different voltage sweep rates is evidenced from Figure 2c, which shows LSV obtained at sweep rates ranging from 0.01 to 0.2 $V{\cdot}s^{-1}$ in 0.3 M oxalic acid electrolyte with 5 vol % ethanol. The nonreversible formation of a porous AAO layer onto the anode surface affects ion transport to the reaction interface, decreasing both the anodic current density and V_{HA} value as the sweep rate is reduced. Despite these differences, all of the LSV curves display features similar to those discussed for Figure 2a, except for the curve corresponding to a sweep rate of 0.2 $V{\cdot}s^{-1}$, which shows a V_{BD} voltage of 138 V, noticeably smaller than that of the curves recorded at slower voltage sweep rates, indicating that low sweep rates are more adequate to study HA processes.

Table 1. Characteristic Values of V_{HA}, V_{BD}, and Voltage Range of the B* Plateau Interval, Obtained from LSV in Oxalic Acid Electrolytes with Concentrations Ranging from 0.075 to 0.300 M, Containing 5−10 vol. % Ethanol

$[(COOH)_2]$ (M)	ethanol (vol %)	V_{HA} (V)	B^* range (V)	V_{BD} (V)
0.300 ± 0.002	5.0 ± 0.1	100 ± 1	120−150	153 ± 1
0.150 ± 0.002	5.0 ± 0.1	106 ± 1	150−170	175 ± 1
0.100 ± 0.002	10.0 ± 0.1	112 ± 1	160−190	190 ± 1
0.075 ± 0.002	10.0 ± 0.1	114 ± 1	190−225	226 ± 1

In both, Table 1 and Figure 2b, the influence of the oxalic acid concentration on the $j_A(V_{an})$ curves can be observed. The voltage value of V_{HA} (i.e., the value of the anodic voltage at which the HA regime starts) shifts to higher anodic voltages as the oxalic acid concentration decreases. A similar trend can be also observed for the other characteristic parameters, B^* and V_{BD}. Additionally, the anodic current density for a given anodic voltage decreases as the oxalic acid concentration is reduced. These observations indicate that the behavior of Al anodic oxidation and particularly that of the HA regime can be controlled by carefully selecting the electrolyte oxalic acid concentration.

Mechanism of Hard Anodization Processes. As it has been previously mentioned, HA of Al is generally ascribed to a diffusion-limited process due to the increased diffusion length of the ionic species involved in the anodic electrochemical reactions, as a consequence of the fast growth rate exhibited by H-AAO membranes.[2−4] On the contrary, the growth of the AAO membrane during the MA process, is usually slower. Therefore, no limited diffusion regime is established for any of the ionic species involved in the MA electrochemical reactions. The ionic flux through a nanoporous membrane of porosity P and thickness L is given by the extended Nernst−Planck equation for the ionic transport (eq 2).[44−46]

$$J = -PD\frac{\partial C(x)}{\partial x} - \frac{zFP}{RT}DC(x)\frac{\partial V(x)}{\partial x} + PC(x)v_{eo}(x); \quad (0 \le x \le L) \quad (2)$$

where x represents the distance to the reaction interface, that is, to the pore bottom, D is the diffusion coefficient of the specific ion of interest, and $C(x)$ corresponds to its concentration and z to its charge number. R and F are ideal gas and Faraday constants, respectively, $V(x)$ is the electric potential inside the pores and v_{eo} is the solution velocity due to convection. The first, second, and third terms in eq 2 correspond to diffusion, migration, and convection contributions to ionic transport, respectively. Despite the high stirring rates employed in our experiments, which cause intense forced convection in the bulk of the electrolyte, as a first approximation the contribution of this term inside the pore channels ($0 \le x \le L$) is considered to be negligible due to electrolyte confinement in the nanoporous medium. Furthermore, the presence of high mobility H^+ ions assures the high electric conductivity of the electrolyte. Therefore, the electric potential drop through the pore

DOI: 10.1021/acsami.5b10712
ACS Appl. Mater. Interfaces XXXX, XXX, XXX−XXX

channels is considered to be small in comparison with that at the bottom of the pores due to the highly resistive alumina barrier layer.[20,47,48] Therefore, migration is neglected, and only the first term in eq 2, associated with diffusion contribution to ion transport, will be considered in our simple model.

Assuming that the electrolyte ions exhibit a linear diffusion profile along a constant concentration gradient between the pore bottom and the bulk of the electrolyte (see Figure 3a), the ion concentration can then be written as $C(x) = C(0) + [C(L) - C(0)]x/L$.

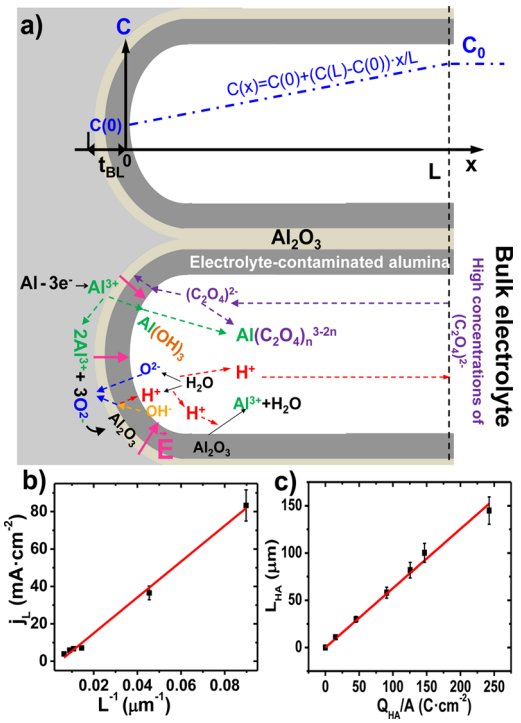

Figure 3. (a) Schematic diagram of the chemical and electrochemical reactions taking place during aluminum anodization in oxalic acid electrolytes (lower pore), and linear profile of the concentration gradient (upper pore) along the pore length. (b) Fitting of the final anodization current density, j_L, as a function of the inverse of the total membrane thickness, L, obtained for H-AAO samples anodized at 120 V in 0.300 M oxalic acid electrolyte. (c) Thickness of H-AAO layers, L_{HA}, grown by anodization in 0.3 M oxalic acid at 120 V, as a function of the HA charge density, Q_{HA}/A, A being the area of the aluminum electrode.

If the electrochemical reaction is limited by the transport of ions from the electrolyte, we can state that the concentration of these particular ions at the reaction interface is negligible, and therefore $C(0) = 0$, while $C(L)$ can be assumed to be equal to the initial concentration of the bulk electrolyte, C_0, kept constant by the vigorous stirring employed during the whole anodization process. Thus, the diffusion-limited current density, j_{DL}, can be approximated by eq 3.

$$j_{DL} = |zFJ| = \frac{zPFDC_0}{L} \quad (3)$$

Therefore, a diffusion-limited mechanism will be associated with an inverse dependence of the anodization current density on the membrane thickness. It is worth mentioning that more sophisticated models that include a nonzero but constant electric field within the pore channels (Goldman constant-field approximation)[49] would also result in an inverse relationship between the anodization current density and the membrane thickness for the case of diffusion-limited electrochemical reactions.[50]

In order to verify whether or not this is the actual behavior of the HA current transients, a series of samples were fabricated in oxalic acid 0.300 M containing 5 vol % of ethanol, at an HA voltage of 120 V (voltage sweep rate of 0.2 V·s^{-1}). Different time interval durations of the potentiostatic HA step varying from 0 s up to 36000 s were employed. The final anodization current density (that is, the last current density value recorded during the anodization), henceforth called j_L, is depicted in Figure 3b as a function of the inverse of the total AAO membrane thickness measured from SEM images. A linear dependence of j_L on L^{-1} is clearly observed, demonstrating that HA can be considered as a diffusion controlled process, and hence, $j_A = j_{DL}$. Therefore, we can ascribe the local maximum in the $j_A(V_{an})$ curve of Figure 2a as the beginning point of the HA regime, characterized by a diffusion-limited oxide growth. Figure 3c shows the dependence of the H-AAO layer thickness on the charge density flowing through the electrochemical cell during HA process, evidencing a linear relationship despite the nonconstant growth rate of H-AAO layers on time previously mentioned and illustrated in Figure S1.

From the previous results, a diffusion-limited mechanism has been demonstrated to dominate the anodic oxidation of Al during HA processes. However, it is still unclear which one of the ions involved in the anodic oxidation of Al is depleted at the reaction interface, thus limiting the anodization process. The overall anodic reaction occurring during the oxidation of aluminum is given by[20,51]

$$2Al + 3H_2O \rightarrow Al_2O_3 + 6H^+ + 6e^- \quad (4)$$

This global anodic reaction results from the different chemical and electrochemical reactions that take place at the metal/oxide (m/o) and oxide/electrolyte (o/e) interfaces, which are schematized in Figure 3a. At the m/o interface, metallic aluminum is oxidized to Al^{3+} ions. Around 60% of the Al^{3+} ions react with O^{2-} anions extracted from the electrolyte at the o/e interface that reach the m/o interface by ionic migration across the alumina barrier layer, as a consequence of the intense electric field.[20,52,53] This reaction leads to the formation of Al_2O_3 at the m/o interface, thus increasing the barrier layer thickness. The remaining 40% of Al^{3+} ions migrate outward, and finally, they are ejected into the electrolyte at the o/e interface. Depending on the local chemical environment, ejected Al^{3+} ions are complexed by electrolyte anions (i.e., oxalates), forming water-soluble complexes, or they react with OH^- ions leading to the formation of aluminum hydroxides, which are further hydrolyzed resulting in redeposition of alumina at the o/e interface.[52,54,55] The Al_2O_3 formation at the o/e interface plays an important role in the growth of barrier-type alumina layers. However, if this phenomenon is absent or reduced to an extent, alumina films develop a porous structure.[20,52,56,57] Additionally, chemical dissolution of alumina takes place also in the o/e interface.[58−60]

From all of the above-discussed chemical and electrochemical reactions, we can assume that the most probable ion to be depleted at the reaction o/e interface is the oxalate ion. The rest of the ions can be discarded since O^{2-}, OH^-, and H^+ ions are continuously generated from water molecules at this interface, and thus, they are unlikely to be depleted. In the same way, water is the most abundant chemical species in the

DOI: 10.1021/acsami.5b10712
ACS Appl. Mater. Interfaces XXXX, XXX, XXX−XXX

electrolyte since it is the solvent, while the Al substrate assures a continuous supply of Al^{3+} ions. Additionally, the oxalate ions play a crucial role in the development of nanoporous structures during the electrochemical anodization of Al, even though they are not directly involved in the electrochemical oxidation of aluminum. In oxalic acid electrolytes, the fraction of Al^{3+} ions that are ejected into the electrolyte as a consequence of the field-driven ionic migration across the alumina barrier layer are complexed by oxalate ions forming water-soluble molecules. In a similar way, phosphate or sulfate ions bind Al^{3+} forming soluble complex ions during Al anodization in phosphoric or sulfuric acids, respectively. Therefore, during the anodization process in pore-forming electrolytes, the growth of the alumina layer takes place mainly at the m/o interface, and the Al^{3+} ions ejected into the electrolyte do not have any important contribution to Al oxide growth. However, in nonpore forming electrolytes, such as borate, the Al^{3+} ions ejected into the electrolyte do not from complexes. Depending on the anodic conditions (pH, temperature, etc.), they lead to the formation of aluminum hydroxides (i.e., $Al(OH)_3$ and $Al(OH_2)_6^{3+}$) which are hydrolyzed forming alumina. As a consequence, Al_2O_3 growth occurs at the same time in both o/e and m/o interfaces.[20,56,61]

Therefore, it is possible to argue that during the HA of Al in oxalic acid electrolytes, a fraction of the ejected Al^{3+} ions react with oxalates at a rate that is determined by the ionic diffusion of oxalate ions from the bulk of the electrolyte to the reaction interface. The rest of Al^{3+} ions or at least a substantial fraction of them react with hydroxides or water, forming nonsoluble chemical species that finally contribute to the formation of Al_2O_3 at the o/e interface. The redeposition of Al_2O_3 at the o/e interface might result in a noticeable thickening of the Al_2O_3 barrier layer at the bottom of the pores and in a decrease of the electric field strength across the barrier layer, given by $\Delta V_{BL}/t_{BL}$, where $\Delta V_{BL} \approx V_{an}$ = cte. The decrease in electric field strength due to barrier thickening is responsible for the progressive diminution of anodization current density and for the nonlinearity of the H-AAO layer with the anodization time shown in Figure S1.

Experimental Validation of the HA Model. In order to verify the proposed mechanism for the HA processes, we have systematically measured the thickness of the alumina barrier layer, t_{BL}, at different time interval durations of the HA potentiostatic step varying from 0 to 36000 s for samples fabricated in 0.300 M oxalic acid containing 5 vol % of ethanol, under an applied anodic voltage of 120 V.

Figure 4a illustrates the dependence of both, the alumina barrier layer thickness and the limit current density, j_L, on the total thickness, L, of the nanoporous alumina membranes. It can be seen that, while t_{BL} increases with the membrane total thickness, j_L decreases. This relationship between j_L and L is in good agreement with eq 1 and therefore with the proposed HA mechanism. In fact, t_{BL} and j_L are closely related, as can be observed in Figure 4b. The limit current density, j_L, shows an exponential dependence on t_{BL} that can be fitted through the following phenomenological equation:

$$j_L \approx 4 \cdot 10^6 \text{ mA cm}^{-2} e^{(13.4\text{nm}/t_{BL})} \quad (5)$$

By comparing eqs 1 and 5, we can see that the current density still follows, in the case of HA processes, the exponential dependence on the barrier layer thickness predicted by the high-field conduction theory for MA,[38] with $j_0 = 4 \times 10^6$ mA cm^{-2} and $\beta = 0.112$ nm·V^{-1}. Therefore, other contributions to the anodic current density, such as electron avalanche multiplication,[20,52] are negligible or play a minor role during HA processes as long as dielectric breakdown of the oxide layer is avoided. Furthermore, the good agreement found between eqs 1 and 5 employing temperature independent fitting parameters points out that the heat generated due to the high anodic current densities is successfully dissipated by the refrigeration system. According to our experimental results, the increase of the porous membrane thickness entails an increase in the diffusion length for the ions, and therefore, the flux of oxalate ions that reach the o/e interface is reduced according to eqs 2 and 3. The change of j_L with the membrane thickness and its dependence on t_{BL} can be understood in the frame of the proposed HA mechanism. The lower the rate at which the oxalate ions reach the o/e interface, the higher the amount of ejected Al^{3+} ions that do not from complexes and hence contribute to the formation of alumina or aluminum hydroxides at this interface, resulting in an increase of t_{BL} and in a reduction of the effective electric field across it. Consequently, the migration of O^{2-} and OH^- across the barrier layer and thus the current density are also reduced, according to eq 1.

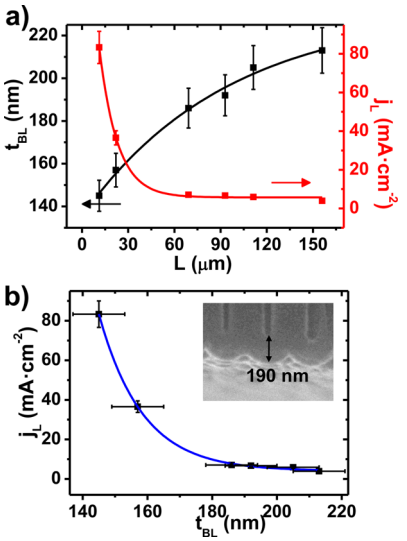

Figure 4. (a) Dependence of the barrier layer thickness, t_{BL}, and limit current density, j_L, on the total thickness of the alumina membrane. (b) Dependence of the limit current density on the alumina barrier layer thickness. The inset shows a SEM image of the alumina barrier layer of the sample anodized during 10800 s. All of the HAs were performed at 120 V in 0.300 M oxalic acid electrolyte containing 5 vol % of ethanol.

Analysis of Interpore Distance, Pore Diameter, and Self-Organization in HA. On the basis of the analysis of SEM bottom views of H-AAO membranes grown in 0.300 M oxalic acid electrolytes at 120 V (Figure 5), we have studied the variation of the interpore distance as well as the evolution of the pore self-organization with the time duration of the anodization process. The pore ordering degree in the HA-AAO layer is low at the beginning of the potentiostatic HA process, as can be seen in Figure 5a. However, the pore distribution rapidly achieves a highly ordered hexagonal pore arrangement that holds for HA durations between 5 and 240 min (Figures 5b–e).

Finally, for very long HA process (Figure 5f) the pore arrangement turns into a randomly distributed form. The

DOI: 10.1021/acsami.5b10712
ACS Appl. Mater. Interfaces XXXX, XXX, XXX−XXX

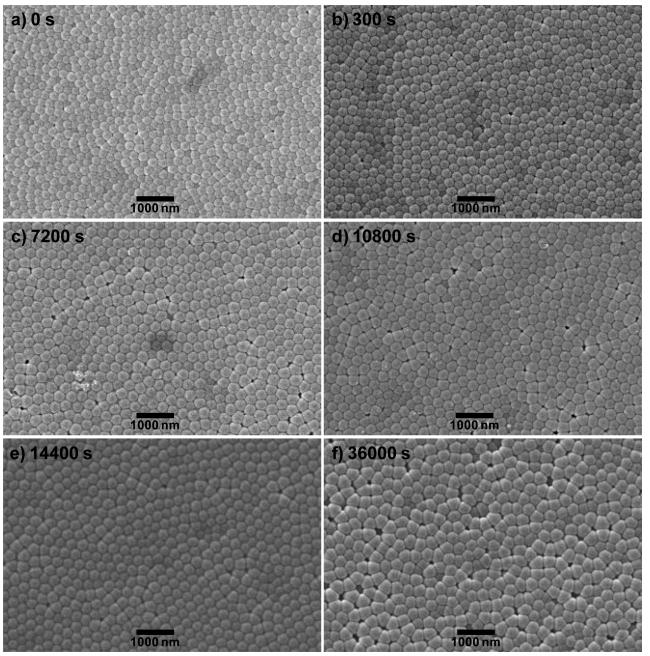

Figure 5. SEM images of the pore bottom of H-AAO membranes synthesized at 120 V in oxalic acid 0.300 M electrolytes containing 5 vol % of ethanol, during different anodization times, ranging from 0 to 36000 s.

reduction of the nanopore self-ordering degree can be attributed to the decrease of both, the electric field strength and its spatial distribution gradient, as a consequence of the increased barrier layer thickness in thick H-AAO layers, therefore resulting in a decrease of the anodization current density, as experimentally measured. This behavior is similar to that reported for M-AAO films, in which the ordering degree of the nanopore arrangement first increases due to self-ordering phenomena,[5,60] but afterward, it decreases again for long time duration anodization processes.[42]

The change of the interpore distance, D_{int}, with the final anodization current density, j_L, during HA is plotted in Figure 6a. These results indicate that D_{int} does not remain constant during the whole HA process but that it decreases exponentially with j_L, in good agreement with previous works.[10,20,23,61] Therefore, contrary to the case of MA, the ratio D_{int}/V_{an} is not constant during HA processes, taking values close to 2 nm·V^{-1} for high j_L but increasing up to 2.7 nm·V^{-1} as the final anodization current density is reduced during long HA steps.

The variation of D_{int} can be related to the thickening of t_{BL} with the anodization time as a result of the depletion of oxalate ions in HA processes. Indeed, in the frame of the viscous-flow model for the growth of nanoporous alumina,[62,63] D_{int} has been predicted to be proportional to $t_{BL}^{3/2}/V_{an}$ (see Supporting Information). Figure 6b plots D_{int} against $t_{BL}^{3/2}/V_{an}$, indicating that the experimental data can be well fitted by a linear equation with a slope of 7.3 V·nm$^{-1/2}$. This value is in good agreement with the viscous-flow model, which postulates an electrostatic energy-induced surface instability as the mechanism controlling pore interspacing in anodic oxide films (see discussion in Supporting Information). Despite this remarkable good agreement between the experimental data and predictions coming from this last theory, to favor unambiguously the viscous-flow model against the field-assisted dissolution one is not possible with the available data.

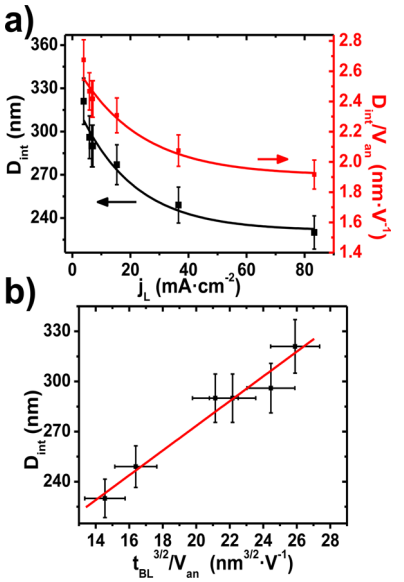

Figure 6. (a) Dependence of the interpore distance, D_{int}, and the ratio of the interpore distance to anodizing voltage, D_{int}/V_{an}, on the limit current density, j_L, for H-AAO membranes anodized at 120 V in 0.300 M oxalic acid containing 5 vol % of ethanol. (b) Variation of D_{int} against $t_{BL}^{3/2}/V_{an}$ for the same set of samples.

A comparison of TEM studies for both MA and HA-AAO membranes, performed after reducing the sample thickness by ion-milling thinning, is presented in Figure 7. The morpho-

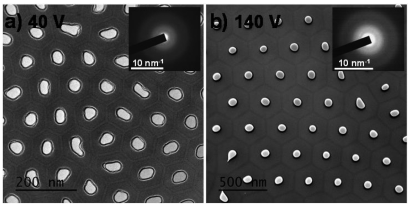

Figure 7. TEM images of AAO membranes fabricated in 0.300 M oxalic acid electrolytes. (a) M-AAO, anodized at 40 V. (b) H-AAO, anodized at 140 V. The respective insets show the SAED spectra of each sample.

logical structure of both types of membranes is similar, and it is characterized by the self-ordered hexagonal pore arrangement. Furthermore, the presence of two alumina layers is observed: a contaminated alumina layer located in the region adjacent to the pores, and a purer alumina layer placed in between of two adjacent pores. In both cases, an amorphous structure is evidenced by the respective selected area electron diffraction (SAED) images displayed as insets in Figure 7.[64−66] However, a clear difference in the ratio of pore diameter, D_p, to D_{int} can be observed when comparing M-AAO and H-AAO membranes. While M-AAO have large pores in comparison to the interpore distance, thus resulting in an average D_p/D_{int} ratio of 0.35, H-AAO membranes present relatively narrow pores separated by larger distances, thus resulting an averaged ratio of 0.23. This reduction in the D_p to D_{int} ratio also implies lower porosity values in H-AAO than those found in M-AAO membranes fabricated under self-ordering conditions, in good agreement with previous studies.[2,20,42] The pore diameter shrinking with respect to the interpore distance observed in H-AAO membranes could also be related to the formation of an

DOI: 10.1021/acsami.5b10712
ACS Appl. Mater. Interfaces XXXX, XXX, XXX−XXX

alumina layer in the o/e interface as a consequence of the depletion of oxalate ions in the pore bottom. Therefore, it is consistent with the proposed diffusion limited mechanism as the characteristic feature of HA processes.

The fact that HA is a diffusion-limited process and that therefore the concentration of reactive chemical species at the o/e interface is negligible suggests that the concentration of oxalic acid in the bulk of the electrolyte should not be a key factor governing the self-ordering of the nanopores in H-AAO membranes. This is a remarkable difference with the case of M-AAO ones, where highly ordered porous arrangements have been obtained only in a limited number of electrolytes and in a relatively narrow range of concentrations and applied anodic potentials for each specific electrolyte.[43,66] This fact motivated a study of the self-ordering regimes during HA of Al that will be discussed in the following section.

Establishment of Self-Ordering Regimes in Hard Anodization of Aluminum through Voltammetric Studies. On the basis of the voltammograms obtained for oxalic acid electrolytes with different concentrations, we have synthesized a set of H-AAO membranes covering the whole voltage range comprising V_{HA} and V_{BD} for each electrolyte (see Table 1). In order to verify the self-ordered spatial arrangement of the nanopores grown during HA processes, the back of the alumina membranes was checked by SEM, after removing the aluminum substrate and the alumina barrier layer occluding the pore channels. Image analysis, performed by employing self-correlation function[35,36] allows us to determine the best self-ordering conditions for each electrolyte. The complete batch of samples fabricated in 0.150 M oxalic acid electrolyte containing 5 vol % of ethanol at HA voltages ranging from 120 to 170 V, is shown in Figure S2 (see Supporting Information).

Even though all samples exhibit short-range porous spatial self-ordering, the larger self-ordered pore domains (size around 12 μm^2) with hexagonal symmetry are found for the sample synthesized at 170 V. A similar study was performed for all samples anodized during 1.5 h at voltages ranging from 100 to 225 V in 0.075−0.300 M oxalic acid electrolytes containing 5−10 vol % of ethanol, and some selected bottom-view SEM images are shown in Figure 8.

Figure 8a corresponds to a bottom-view of a H-AAO membrane obtained by hard anodization in 0.300 M oxalic acid electrolyte at 100 V, which corresponds to the V_{HA} value for this electrolyte (see Figure 2b. At this value of the anodization voltage, close to the beginning of the HA regime, the pores follow a random distribution at the bottom surface of the alumina membrane. The spatial ordering degree of the nanopore arrangement is clearly improved by increasing the anodization voltage, as can be seen in the micrographs of Figure 8b and c, obtained at 130 and 150 V, respectively. Similar results were obtained for all the electrolytes with different oxalic acid concentrations studied in this work (see Figure 8d−f). For all of them, it was possible to find an interval of HA voltages at which the nanopores exhibit a self-ordered spatial distribution with hexagonal symmetry. At the same time, if the HA voltages are too near to the V_{HA} value for a given oxalic acid concentration, the hard-anodic samples exhibit worse pores ordering than those obtained at higher anodization voltages, much closer to V_{BD}. Therefore, a good spatial ordering degree of the nanopores can be achieved when $V_{HA} \ll V_{an} < V_{BD}$, in good agreement with previous works that reported pore self-organization for anodization voltages close to the breakdown potential.[1,67,68]

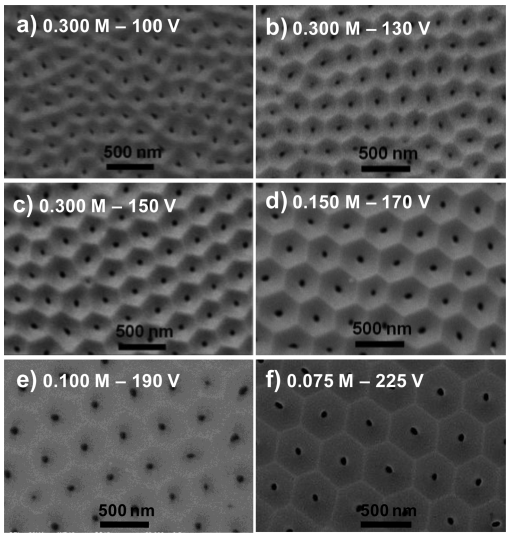

Figure 8. SEM images at the bottom surface of H-AAO membranes synthesized by hard anodization in oxalic acid electrolytes with different acidic concentrations and under different anodization voltages of (a) 100 V, 0.300 M; (b) 130 V, 0.300 M; (c) 150 V, 0.300 M; (d) 170 V, 0.150 M; (e) 190 V, 0.100 M; and (f) 225 V, 0.075 M.

By correlating the given voltage values for the B^* interval in Table 1 with the SEM images of Figure 8, it can be seen that pore self-ordering conditions for each electrolyte were obtained at a certain HA voltage value that fits into the B^* range. In other words, the HA voltages leading to spatially self-ordered pore growth for all the tested oxalic acid concentrations fall into the plateau observed in the respective voltammograms (see Figure 3). In addition, our method based on voltammetric studies of the anodic oxidation of Al for the determination of the self-ordering HA conditions can be extended to other electrolytes, such as oxalic acid electrolytes containing ethylene glycol as an additive, as explained in detail in the Supporting Information and illustrated in Figure S3, which are interesting due to their stabilizing effect in the HA processes.

The reason for the correspondence between the current plateau observed in the voltammograms and the spatial self-ordering of the nanopores during HA processes remains still not fully understood. It could be related to a current compensation by the increase of the effective reaction surface, as a consequence of the formation of dissipative structures as proposed by Pashchanka and Schneider.[69,70] This phenomenon may be responsible for pore rearrangement following a hexagonally centered structure that maximizes the packing density of the nanopores.

The dependence of the interpore distance, pore diameter, and porosity on the HA voltage for all the self-ordered H-AAO membranes studied in this section is shown in Figure 9a. Figure 9b depicts the dependence of the alumina barrier layer thickness on V_{an}. A linear relationship of both D_{int} and t_{BL} on the anodization voltage was found for these samples, anodized under HA conditions during 1.5 h, resulting in proportionality constants of about 2.4 nm·V^{-1} and 1.1 nm·V^{-1} for D_{int} and t_{BL}, respectively. It is worth mentioning that the linear relationship between D_{int} and t_{BL} on the anodization voltage is only obtained under particular experimental conditions, in view that both geometrical parameters of H-AAO membranes depend not only on the anodization voltage but also on the anodization

DOI: 10.1021/acsami.5b10712
ACS Appl. Mater. Interfaces XXXX, XXX, XXX−XXX

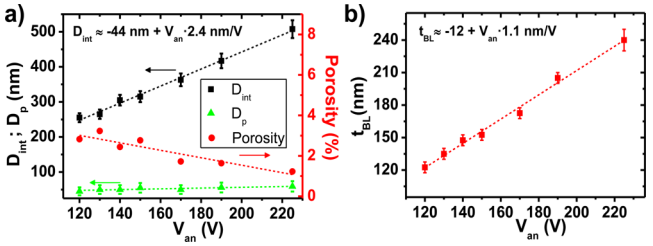

Figure 9. (a) Dependence of the interpore distance, D_{int}, pore diameter, D_p, and estimated porosity on the hard anodization voltage for H-AAO membranes obtained in oxalic acid electrolytes with concentrations ranging from 0.075 to 0.300 M. (b) Dependence of the alumina barrier layer thickness, t_{BL}, on the anodization voltage for the same H-AAO membranes presented in panel a. The solid data-points represent experimental values, whereas the dashed lines represent the respective linear fits of the experimental data.

time and membrane thickness, as previously discussed. Therefore, the different proportionality constants between D_{int} and V_{an} reported in the literature[2,8,10,20] can be ascribed to different membrane thicknesses and experimental synthesis conditions employed in these works.

Despite the remarkable large and continuous variation in D_{int} and t_{BL} with V_{an}, D_p keeps at an almost constant value of around 50−60 nm for all of the H-AAO membranes studied here. As can be observed in Figure 9a, the independence of pore diameter, D_p, on the anodization voltage allows one to modify the porosity of the H-AAO layers, estimated as $P = 100 \cdot (\pi/2) \cdot 3^{-1/2} \cdot (D_p/D_{int})^2$,[42] while keeping the good ordering degree of the nanopores, contrary to the case of M-AAO for which the porosity is limited to values of about 10%[42] or higher, if it is desired to keep the spatial nanopores ordering of the alumina membrane. This novel finding provides additional flexibility for the design of tailored nanoporous membranes for their use as templates, allowing for the independent tuning of pore diameter and interpore distance.

It is worth noting that the quest for the self-ordering regimes during Al anodization is usually performed by trial and error methods, which is time-consuming and expensive. The method presented here allows one to perform a preliminary selection of the anodic conditions, appropriately chosen from the study of the LSV curves, which can lead to an optimum self-ordered nanopore arrangement for a given electrolyte concentration. Therefore, this approach results in a more efficient and time-saving fabrication technique.

CONCLUSIONS

The anodic oxidation of Al under HA conditions in oxalic acid electrolytes with different concentrations has been studied in detail by performing LSV experiments and systematic characterization of the morphological parameters of H-AAO (D_{int}, D_p, and t_{BL}) and their variation as a function of the HA membrane thickness and the anodization current density. The results allow us to conclude that HA processes in oxalic acid electrolytes are mainly governed by the diffusion of oxalate ions through the pore channels from the bulk of the electrolyte to the pore bottom, according with our phenomenological model. The depletion of oxalates at the bottom of the pores causes an increase of the alumina barrier layer thickness due to the redeposition of the Al^{3+} ions ejected into the electrolyte during Al anodization, which, in the case of HA processes, contributes to the growth of alumina in the oxide/electrolyte interface. This fact might be the key difference between the MA and the HA regimes.

The study of HA processes in electrolytes with different oxalic acid concentrations for a wide variety of anodization voltages allowed us to determine the best self-ordering conditions for each electrolyte concentration that give rise to highly ordered spatial distributions of pores during HA processes. Our results indicate that, by carefully adjusting the conditions of the HA processes, it is possible to produce hexagonally self-ordered nanopore arrangements exhibiting a large range of available interpore distances (240−507 nm), while keeping the pore diameter almost constant (50−60 nm), thus allowing for a continuous tuning of the membrane porosity.

Additionally, voltammetric analysis of the anodic oxidation of Al, which has been applied to the HA of Al for the first time in this work to the best of our knowledge, allows us to distinguish from the mild and the hard anodization regimes for any electrolyte. Furthermore, the correspondence found between the self-ordering anodization voltage and the current plateau observed in the LSV for each one of the different electrolytes tested in this work provides a powerful method to determine, in a time-saving manner, the HA conditions that might lead to highly spatially ordered nanoporous arrangements. This method was also successfully applied to an electrolyte composed of 0.300 M oxalic acid and 50 vol % of ethylene glycol, thus demonstrating its flexibility of implementation in other electrolytes and paving the way for extensive research of the pores self-ordering conditions in more complex electrolytes. Furthermore, our study may open the door for innovative anodization protocols allowing for the preparation of H-AAO membranes keeping constant pore density values, by controlling the anodization parameters and electrolyte concentration, in order to compensate for the diffusion length increase due to the fast growth of H-AAO membranes.

ASSOCIATED CONTENT

Supporting Information

The Supporting Information is available free of charge on the ACS Publications website at DOI: 10.1021/acsami.5b10712.

Additional experimental results and discussions (PDF)

AUTHOR INFORMATION

Corresponding Author

*E-mail: vegavictor@uniovi.es.

Present Address

[⊥]J.G.: IFW Dresden, Institute for Metallic Materials, P.O. Box 270116, D-01171 Dresden, Germany.

Notes

The authors declare no competing financial interest.

ACKNOWLEDGMENTS

Financial support under Spanish MINECO research Projects MAT2013-48054-C2-2-R and MAT2013-47231-C2-1-P, and Consejería de Economía y Empleo from Principality of Asturias and FICyT under Project No. GIC-FC-15-GRUPIN14-085 is acknowledged. V.V. thanks DAAD (PKZ A/09/95123) and University of Oviedo for the respective internship grants. J.G. thanks FICYT for his "Severo Ochoa" fellowship (BP10-035). Scientific support from the University of Oviedo SCT's is also gratefully recognized.

DOI: 10.1021/acsami.5b10712
ACS Appl. Mater. Interfaces XXXX, XXX, XXX−XXX

REFERENCES

(1) Chu, S. Z.; Wada, K.; Inoue, S.; Isogai, M.; Yasumori, A. Fabrication of Ideally Ordered Nanoporous Alumina Films and Integrated Alumina Nanotube Arrays by High Field Anodization. *Adv. Mater.* **2005**, *17*, 2115−2119.

(2) Lee, W.; Ji, R.; Gösele, U.; Nielsch, K. Fast Fabrication of Long-Range Ordered Porous Alumina Membranes by Hard Anodization. *Nat. Mater.* **2006**, *5*, 741−747.

(3) Ha, Y. C.; Jeong, D. Y. Fast Fabrication of a High-aspect-ratio, Self-ordered Nanoporous Alumina Membrane by Using High-field Anodization. *J. Korean Phys. Soc.* **2010**, *57*, 1661−1666.

(4) Santos, A.; Montero-Moreno, J. M.; Bachmann, J.; Nielsch, K.; Formentín, P.; Ferré-Borrull, J.; Pallarés, J.; Marsal, L. F. Understanding Pore Rearrangement during Mild to Hard Transition in Bilayered Porous Anodic Alumina Membranes. *ACS Appl. Mater. Interfaces* **2011**, *3*, 1925−1932.

(5) Masuda, H.; Fukuda, K. Ordered Metal Nanohole Arrays Made by a Two-Step Replication of Honeycomb Structures of Anodic Alumina. *Science* **1995**, *268*, 1466−1468.

(6) Santos, A.; Formentín, P.; Ferré-Borrull, J.; Pallarès, J.; Marsal, L. F. Nanoporous Anodic Alumina Obtained without Protective Oxide Layer by Hard Anodization. *Mater. Lett.* **2012**, *67*, 296−299.

(7) Norek, M.; Dopierała, M.; Stępniowski, W. J. Ethanol Influence on Arrangement and Geometrical Parameters of Aluminum Concaves Prepared in a Modified Hard Anodization for Fabrication of Highly Ordered Nanoporous Alumina. *J. Electroanal. Chem.* **2015**, *750*, 79−88.

(8) Li, Y. B.; Zheng, M. J.; Ma, L. High-Speed Growth and Photoluminescence of Porous Anodic Alumina Films with Controllable Interpore Distances Over a Large Range. *Appl. Phys. Lett.* **2007**, *91*, 073109.

(9) Yi, L.; Zhiyuan, L.; Shuoshuo, C.; Xing, H.; Xinhua, H. Novel AAO Films and Hollow Nanostructures Fabricated by Ultra-High Voltage Hard Anodization. *Chem. Commun.* **2010**, *46*, 309−311.

(10) Li, Y. B.; Zheng, M.; Ma, L.; Shen, W. Fabrication of Highly Ordered Nanoporous Alumina Films by Stable High-Field Anodization. *Nanotechnology* **2006**, *17*, 5101−5105.

(11) Montero-Moreno, J. M.; Waleczek, M.; Martens, S.; Zierold, R.; Görlitz, D.; Vega Martínez, V.; Prida, V. M.; Nielsch, K. Constrained Order in Nanoporous Alumina with High Aspect Ratio: Smart Combination of Interference Lithography and Hard Anodization. *Adv. Funct. Mater.* **2014**, *24*, 1857−1863.

(12) Lee, W.; Scholz, R.; Gösele, U. A Continuous Process for Structurally Well-Defined Al_2O_3 Nanotubes Based on Pulse Anodization of Aluminum. *Nano Lett.* **2008**, *8*, 2155−2160.

(13) Lee, W.; Schwirn, K.; Steinhart, M.; Pippel, E.; Scholz, R.; Gösele, U. Structural Engineering of Nanoporous Anodic Aluminium Oxide by Pulse Anodization of Aluminium. *Nat. Nanotechnol.* **2008**, *3*, 234−239.

(14) Pitzschel, K.; Montero-Moreno, J. M.; Escrig, J.; Albrecht, O.; Nielsch, K.; Bachmann, J. Controlled Introduction of Diameter Modulations in Arrayed Magnetic Iron Oxide Nanotubes. *ACS Nano* **2009**, *3*, 3463−3468.

(15) Lee, W.; Kim, J. C.; Gösele, U. Spontaneous Current Oscillations during Hard Anodization of Aluminum under Potentiostatic Conditions. *Adv. Funct. Mater.* **2010**, *20*, 21−27.

(16) Pitzschel, K.; Bachmann, J.; Martens, S.; Montero Moreno, J. M.; Kimling, J.; Meier, G.; Escrig, J.; Nielsch, K.; Gorlitz, D. Magnetic Reversal of Cylindrical Nickel Nanowires with Modulated Diameters. *J. Appl. Phys.* **2011**, *109*, 033907.

(17) Li, J.; Li, C.; Chen, C.; Hao, Q.; Wang, Z.; Zhu, J.; Gao, X. Facile Method for Modulating the Profiles and Periods of Self-Ordered Three-Dimensional Alumina Taper-Nanopores. *ACS Appl. Mater. Interfaces* **2012**, *4*, 5678−5683.

(18) Vega, V.; Böhnert, T.; Martens, S.; Waleczek, M.; Montero-Moreno, J. M.; Görlitz, D.; Prida, V. M.; Nielsch, K. Tuning the Magnetic Anisotropy of Co-Ni Nanowires: Comparison Between Single Nanowires and Nanowire Arrays in Hard-Anodic Aluminum Oxide Membranes. *Nanotechnology* **2012**, *23*, 465709.

(19) Liu, J.; Liu, S.; Zhou, H.; Xie, C.; Huang, Z.; Fu, C.; Kuang, Y. Preparation of Self-Ordered Nanoporous Anodic Aluminum Oxide Membranes by Combination of Hard Anodization and Mild Anodization. *Thin Solid Films* **2014**, *552*, 75−81.

(20) Lee, W.; Park, S.-J. Porous Anodic Aluminum Oxide: Anodization and Templated Synthesis of Functional Nanostructures. *Chem. Rev.* **2014**, *114*, 7487−7556.

(21) Martín, J.; Martín-González, M.; Fernández, J. F.; Caballero-Calero, O. Ordered Three-Dimensional Interconnected Nanoarchitectures in Anodic Porous Alumina. *Nat. Commun.* **2014**, *5*, 5130.

(22) Almasi Kashi, M.; Ramazani, A.; Noormohammadi, M.; Zarei, M.; Marashi, P. Optimum Self-Ordered Nanopore Arrays with 130−270 nm Interpore Distances Formed by Hard Anodization in Sulfuric/Oxalic Acid Mixtures. *J. Phys. D: Appl. Phys.* **2007**, *40*, 7032−7040.

(23) Li, Y. B.; Ling, Z. Y.; Chen, S. S.; Wang, J. C. Fabrication of Novel Porous Anodic Alumina Membranes by Two-Step Hard Anodization. *Nanotechnology* **2008**, *19*, 225604.

(24) Sun, C.; Luo, J.; Wu, L.; Zhang, J. Self-Ordered Anodic Alumina with Continuously Tunable Pore Intervals from 410 to 530 nm. *ACS Appl. Mater. Interfaces* **2010**, *2*, 1299−1302.

(25) Adiga, S. P.; Jin, C.; Curtiss, L. A.; Monteiro-Riviere, N. A.; Narayan, R. J. Nanoporous Membranes for Medical and Biological Applications. *Wiley Interdiscip. Rev.: Nanomed. Nanobiotechnol.* **2009**, *1*, 568−581.

(26) Santos, A.; Macías, G.; Ferré-Borrull, J.; Pallarès, J.; Marsal, L. F. Photoluminescent Enzymatic Sensor Based on Nanoporous Anodic Alumina. *ACS Appl. Mater. Interfaces* **2012**, *4*, 3584−3588.

(27) Kumeria, T.; Rahman, M. M.; Santos, A.; Ferré-Borrull, J.; Marsal, L. F.; Losic, D. Nanoporous Anodic Alumina Rugate Filters for Sensing of Ionic Mercury: Toward Environmental Point-of-Analysis Systems. *ACS Appl. Mater. Interfaces* **2014**, *6*, 12971−12978.

(28) Chen, Y.; Santos, A.; Wang, Y.; Kumeria, T.; Li, J.; Wang, C.; Losic, D. Biomimetic Nanoporous Anodic Alumina Distributed Bragg Reflectors in the Form of Films and Microsized Particles for Sensing Applications. *ACS Appl. Mater. Interfaces* **2015**, *7*, 19816−19824.

(29) Romero, V.; Vega, V.; García, J.; Zierold, R.; Nielsch, K.; Prida, V. M.; Hernando, B.; Benavente, J. Changes in Morphology and Ionic Transport Induced by ALD SiO_2 Coating of Nanoporous Alumina Membranes. *ACS Appl. Mater. Interfaces* **2013**, *5*, 3556−3564.

(30) Law, C. S.; Santos, A.; Kumeria, T.; Losic, D. Engineered Therapeutic-Releasing Nanoporous AnodicAlumina-Aluminum Wires with Extended Release of Therapeutics. *ACS Appl. Mater. Interfaces* **2015**, *7*, 3846−3853.

(31) Vengatesh, P.; Kulandainathan, M. A. Hierarchically Ordered Self-Lubricating Superhydrophobic Anodized Aluminum Surfaces with Enhanced Corrosion Resistance. *ACS Appl. Mater. Interfaces* **2015**, *7*, 1516−1526.

(32) Muñoz Rojo, M.; Grauby, S.; Rampnoux, J.-M.; Caballero-Calero, O.; Martin-Gonzalez, M.; Dilhaire, S. Fabrication of Bi_2Te_3 Nanowire Arrays and Thermal Conductivity Measurement by 3ω-Scanning Thermal Microscopy. *J. Appl. Phys.* **2013**, *113*, 054308.

(33) Böhnert, T.; Vega, V.; Michel, A.-K.; Prida, V. M.; Nielsch, K. Magneto-Thermopower and Magnetoresistance of Single Co-Ni Alloy Nanowires. *Appl. Phys. Lett.* **2013**, *103*, 092407.

(34) Dudem, B.; Ko, Y. H.; Leem, J. W.; Lee, S. H.; Yu, J. S. Highly Transparent and Flexible Triboelectric Nanogenerators with Sub-wavelength-Architectured Polydimethylsiloxane by a Nanoporous Anodic Aluminum Oxide Template. *ACS Appl. Mater. Interfaces* **2015**, *7*, 20520−20529.

(35) Horcas, I.; Fernandez, R.; Gomez-Rodriguez, J. M.; Colchero, J.; Gomez-Herrero, J.; Baro, A. M. WSXM: a Software for Scanning Probe Microscopy and a Tool for Nanotechnology. *Rev. Sci. Instrum.* **2007**, *78*, 013705.

(36) Mínguez-Bacho, I.; Rodríguez-López, S.; Asenjo, A.; Vázquez, M.; Hernández-Vélez, M. Self-Correlation Function for Determination of Geometrical Parameters in Nanoporous Anodic Alumina Films. *Appl. Phys. A: Mater. Sci. Process.* **2012**, *106*, 105−112.

DOI: 10.1021/acsami.5b10712
ACS Appl. Mater. Interfaces XXXX, XXX, XXX−XXX

(37) Güntherschulze, A.; Betz, H. Die Bewegung der Ionengitter von Isolatoren bei Extremen Elektrischen Feldstärken. *Eur. Phys. J. A* **1934**, *92*, 367−374.
(38) Cabrera, N.; Mott, N. F. Theory of the Oxidation of Metals. *Rep. Prog. Phys.* **1949**, *12*, 163−184.
(39) Diggle, J. W.; Downie, T. C.; Goulding, C. W. Anodic Oxide Films on Aluminum. *Chem. Rev.* **1969**, *69*, 365−405.
(40) Lohrengel, M. M. Thin Anodic Oxide Layers on Aluminium and Other Valve Metals: High-Field Regime. *Mater. Sci. Eng., R* **1993**, *11*, 243−294.
(41) Hoar, T. P.; Yahalom, J. The Initiation of Pores in Anodic Oxide Films Formed on Aluminum in Acid Solutions. *J. Electrochem. Soc.* **1963**, *110*, 614−621.
(42) Nielsch, K.; Choi, J.; Schwirn, K.; Wehrspohn, R. B.; Gösele, U. Self-ordering Regimes of Porous Alumina: The 10% Porosity Rule. *Nano Lett.* **2002**, *2*, 677−680.
(43) Prida, V. M.; Sanz, R.; Vega, V.; Navas, D.; Pirota, K. R.; Asenjo, A.; Hernández-Vélez, M. Hernando, B.; Vázquez, M. In *Encycl. Nanosci. Nanotechnol.*; Nalwa, H. S., Ed.; American Scientific Publishers: Valencia, CA, 2011.
(44) Helfferich, F. *Ion Exchange*; McGraw-Hill Inc.: New York, 1962.
(45) Quenneville, E.; Buschmann, M. D. A Transport Model of Electrolyte Convection Through a Charged Membrane Predicts Generation of Net Charge at Membrane/Electrolyte Interfaces. *J. Membr. Sci.* **2005**, *265*, 60−73.
(46) Nikonenko, V. V.; Lebedev, K. A.; Suleimanov, S. S. Influence of the Convective Term in the Nernst−Planck Equation on Properties of Ion Transport through a Layer of Solution or Membrane. *Russ. J. Electrochem.* **2009**, *45*, 160−169.
(47) Yasuda, K.; Schmuki, P. Control of Morphology and Composition of Self-Organized Zirconium Titanate Nanotubes Formed in $(NH_4)_2SO_4/NH_4F$ Electrolytes. *Electrochim. Acta* **2007**, *52*, 4053−4061.
(48) Stanton, L. G.; Golovin, A. A. Effect of Ion Migration on the Self-Assembly of Porous Nanostructures in Anodic Oxides. *Phys. Rev. B: Condens. Matter Mater. Phys.* **2009**, *79*, 035414.
(49) Goldman, D. E. Potential, Impedance and Rectification in Membranes. *J. Gen. Physiol.* **1943**, *27*, 37−60.
(50) Ramírez, P.; Gómez, V.; Cervera, J.; Schiedt, B.; Mafé, S. Ion Transport and Selectivity in Nanopores with Spatially Inhomogeneous Fixed Charge Distributions. *J. Chem. Phys.* **2007**, *126*, 194703.
(51) Alwitt, R. S. In *Electrochemistry Encyclopedia*; Nagy, Z., Ed.; The Electrochemical Society, Inc.: Pennington, NJ, 2002. http://knowledge.electrochem.org/encycl/.
(52) Yi, L.; Zhiyuan, L.; Xing, H.; Yisen, L.; Yi, C. Investigation of Intrinsic Mechanisms of Aluminium Anodization Processes by Analyzing the Current Density. *RSC Adv.* **2012**, *2*, 5164−5171.
(53) Skeldon, P.; Thompson, G. E.; Garcia-Vergara, S. J.; Iglesias-Rubianes, L.; Blanco-Pinzon, C. E. A Tracer Study of Porous Anodic Alumina, Electrochem. *Electrochem. Solid-State Lett.* **2006**, *9*, B47−B51.
(54) Patermarakis, G. The Origin of Nucleation and Development of Porous Nanostructure of Anodic Alumina Films. *J. Electroanal. Chem.* **2009**, *635*, 39−50.
(55) Patermarakis, G.; Moussoutzanis, K. Transformation of Porous Structure of Anodic Alumina Films Formed During Galvanostatic Anodising of Aluminium. *J. Electroanal. Chem.* **2011**, *659*, 176−190.
(56) Oh, J.; Thompson, C. V. The Role of Electric Field in Pore Formation During Aluminum Anodization. *Electrochim. Acta* **2011**, *56*, 4044−4051.
(57) Su, Z. X.; Zhou, W. Z. Pore Diameter Control in Anodic Titanium and Aluminium Oxides. *J. Mater. Chem.* **2011**, *21*, 357−362.
(58) Garcia-Vergara, S. J.; Skeldon, P.; Thompson, G. E.; Habazaki, H. A Flow Model of Porous Anodic Film Growth on Aluminium. *Electrochim. Acta* **2006**, *52*, 681−687.
(59) Thompson, G. E. Porous Anodic Alumina: Fabrication, Characterization and Applications. *Thin Solid Films* **1997**, *297*, 192−201.
(60) Li, A.-P.; Müller, F.; Birner, A.; Nielsch, K.; Gösele, U. Fabrication and Microstructuring of Hexagonally Ordered Two-Dimensional Nanopore Arrays in Anodic Alumina. *Adv. Mater.* **1999**, *11*, 483−487.
(61) Yi, L.; Zhiyuan, L.; Xing, H.; Yisen, L.; Yi, C. Formation and Microstructures of Unique Nanoporous AAO Films Fabricated by High Voltage Anodization. *J. Mater. Chem.* **2011**, *21*, 9661−9666.
(62) Barkey, D.; McHugh, J. Pattern Formation in Anodic Aluminum Oxide Growth by Flow Instability and Dynamic Restabilization. *J. Electrochem. Soc.* **2010**, *157*, C388−C391.
(63) Van Overmeere, Q.; Blaffart, F.; Proost, J. What Controls Pore Spacing in Porous Anodic Oxides? *Electrochem. Commun.* **2010**, *12*, 1174−1176.
(64) Thompson, G. E.; Furneaux, R. C.; Wood, G. C.; Richardson, J. A.; Goode, J. S. Nucleation and Growth of Porous Anodic Films on Aluminium. *Nature* **1978**, *272*, 433−435.
(65) Thompson, G. E.; Wood, G. C. *Treatise on Materials Science and Technology*,; Scully, J. C., Ed.; Academic Press: New York, 1983; Vol. *23*, pp 205−329.
(66) Sulka, G. D. In *Nanostructured Materials in Electrochemistry*; Eftekhari, A., Ed.; Wiley-VCH: Weinheim, Germany, 2008; Chapter 1, pp 1−116.
(67) Ono, S.; Saito, M.; Asoh, H. Self-Ordering of Anodic Porous Alumina Induced by Local Current Concentration: Burning, Electrochem. *Electrochem. Solid-State Lett.* **2004**, *7*, B21−B24.
(68) Chu, S. Z.; Wada, K.; Inoue, S.; Isogai, M.; Katsuta, Y.; Yasumori, A. Large-Scale Fabrication of Ordered Nanoporous Alumina Films with Arbitrary Pore Intervals by Critical-Potential Anodization. *J. Electrochem. Soc.* **2006**, *153*, B384−B391.
(69) Pashchanka, M.; Schneider, J. J. Origin of Self-Organisation in Porous Anodic Alumina Films Derived from Analogy with Rayleigh−Bénard Convection Cells. *J. Mater. Chem.* **2011**, *21*, 18761−18767.
(70) Stępniowski, W. J.; Norek, M.; Michalska-Domańska, M.; Forbot, D.; Król, A. Study on the Correlation between Criterion Number Derived from Rayleigh−Bénard Convective Cells and Arrangement of Nanoporous Anodic Aluminum Oxide. *Mater. Lett.* **2014**, *125*, 124−127.

DOI: 10.1021/acsami.5b10712
ACS Appl. Mater. Interfaces XXXX, XXX, XXX−XXX